PAPER

Global analysis of land-use changes in karst areas and the implications for water resources

Jiawen Zhang[1] · Tanja Liesch[1] · Zhao Chen[2] · Nico Goldscheider[1]

Abstract

Karst areas contain valuable groundwater resources and high biodiversity, but are particularly vulnerable to climate change and human impacts. Land-use change is the cause and consequence of global environmental change. The releases of the Climate Change Initiative-Land Cover (CCI-LC) and World Karst Aquifer Map (WOKAM) datasets have made it possible to explore global land-use changes in karst areas. This paper firstly analyses the global karst land-use distribution in 2020, as well as the land-use transition characteristics between 1992 and 2020. Then, two indicators, proportion of land-use change and dominant type of land-use change, are proposed to identify the spatial characteristics of land-use change in global karst areas. Finally, three examples of land-use change in karst areas are analyzed in detail. Land-use types and proportions of the global karst areas from large to small are as follows: forest (31.78%), bare area (27.58%), cropland (19.02%), grassland (10.87%), shrubland (7.21%), wetland (1.67%), ice and snow (1.16%) and urban (0.71%). The total area of global karst land-use change is 1.30 million km^2, about 4.85% of global karst surface. The land-use change trend of global karst is dominated by afforestation, supplemented by scattered urbanization and agricultural reclamation. The tropical climate has a higher intensity of land-use change. Regions of agricultural reclamation are highly consistent with the population density. These results reflect the impact of human activities and climate change on land-use changes in global karst areas, and serve as a basis for further research and planning of land resource management.

Keywords Karst · Global mapping · Land-use change · Satellite imagery · Anthropogenic use

Introduction

Land-use change is an important component (Foley et al. 2005; Turner et al. 2013) and one of the key drivers (Ward et al. 2000) of global environmental change, and it is the result of a combination of driving factors under the human-land relationship (Liu et al. 2003; Meyfroidt et al. 2013). At the same time, land use also has a close relationship to population migration and economic conditions (DeFries 2013); thus, the assessment of land-use changes is important for the effective planning and management of resources. In recent decades, large-scale anthropogenic land-use changes have led to profound changes in the water cycle and have significantly affected the water resources and ecosystem, which in turn have caused changes in groundwater quality and quantity (Grimm et al. 2008; Winkler et al. 2021).

Karst aquifers make important contributions to the water supply of many regions, cities and countries; about 678 million people or 9.2% of the world's population rely on freshwater from karst aquifers (Stevanović 2019). While karst aquifers are essential for water supply, karst areas provide a variety of habitats for many species, including numerous rare and endemic plant and animal species (Goldscheider 2019). At the same time, the karst groundwater system is closely related to the external surface where there can be rapid transformation, so karst aquifers are particularly vulnerable to land-use change and difficult to manage (Nguyet and Goldscheider 2006; Parise et al. 2015; Panagopoulos and Giannika 2022). With the development of the economy and the expansion of population, human behavior, such as the expansion of

✉ Jiawen Zhang
jiawen.zhang@kit.edu

✉ Nico Goldscheider
nico.goldscheider@kit.edu

1 Institute of Applied Geosciences, Division of Hydrogeology, Karlsruhe Institute of Technology (KIT), Kaiserstr. 12, 76131 Karlsruhe, Germany

2 Institute of Groundwater Management, Technical University of Dresden, 01062 Dresden, Germany

cropland, will gradually increase the stress on karst aquifers in terms of groundwater quality and quantity (Hartmann et al. 2014)—for example, the pressure on groundwater quantity caused by the intensification of agriculture and the pressure on groundwater quality caused by the application of pesticides and fertilizers (Foley et al. 2011). At the same time, urbanization is a strong trend of economic development. This trend will inevitably lead to the expansion of urban land use and the growth of urban population. In the process of urbanization, these changes in land use and landscape patterns are the most obvious changes in the karst surface area (Lambin et al. 2001).

Numerous institutions have released global land-use data products that are inconsistent in scale and classification (Grekousis et al. 2015)—e.g., the International Geosphere-Biosphere Programme's Data and Information System land-use cover (IGBP DISCover; Loveland et al. 2000), Global Land Cover 2000 (GLC2000; Bartholome and Belward 2005), Moderate Resolution Imaging Spectroradiometer LAND-COVER (LC) dataset (MCD12; Friedl et al. 2010), GLOBCOVER and Global Map-Global LC dataset (GLCNMO; Tateishi et al. 2011), GlobalLand 30 (Chen et al. 2015). These global land-use products by different institutions are limited by inconsistencies in resolution, time scale and classification systems, making it challenging to compare and combine the data. Difficulties in accurately assessing the impacts of land-use changes and making decisions about land and resource management can result from a lack of clear understanding of trends and patterns (Fuchs et al. 2013; Winkler et al. 2021). To resolve these issues, it is crucial for institutions to adopt a standardized approach to land-use data collection and analysis, using consistent scales and classification systems.

The World Karst Aquifer Map (WOKAM) was completed in 2017, providing a comprehensive description of the global distribution of karst features (Chen et al. 2017b). This release of data offers valuable insights into the distribution of karst aquifers across the world. Moreover, since most of the global karst areas are discontinuous regions (Chen et al. 2017a), land-use analysis in karst regions requires a high resolution relative to global class datasets. The European Space Agency (ESA) released the Climate Change Initiative – Land Cover dataset (CCI-LC; Bontemps et al. 2013) of global land use with a resolution of 300 m and multi-year time series. The CCI-LC dataset allows one to derive absolute areas and areal changes between land uses (Li et al. 2018; Liu et al. 2018).

Most previous studies on karst water resources have only considered land-use change at the catchment scale (Sonter et al. 2014; Misra and Balaji 2015; Chen et al. 2021a, b). It is essential to quantify and understand the spatiotemporal dynamics of global karst land-use change. Such assessment could provide more comprehensive data for global karst change analysis, and contribute to the awareness of

ecological or environmental change by quantifying global karst land-use change characteristics, allowing for a better understanding of global karst land-use change.

This study aims to quantify the spatiotemporal dynamics of land-use change in karst regions at a global scale based on various global geographical information systems (GIS) datasets. It represents the first attempt to combine CCI-LC data and WOKAM data from 1992 to 2020 to identify and quantify the distribution patterns and land-use changes in global karst regions (Goldscheider et al. 2020). The research content of this article is as follows:

1. Summary of the general situation of land-use distribution in global karst areas
2. For each land-use type, analysis of the area changes between 1992 and 2020 and quantification of the global land-use transition
3. Identification of the spatiotemporal dynamics of global karst land-use change

Materials and methods

This project was undertaken using ArcGIS Desktop by ESRI (version 10.8), the coordinate system is Robinson projection, longitude of central meridian 11 °E, spheroid WGS84. The legends, values and areas mentioned in this paper refer to land use on global karst.

Data source and reclassification system

The European Space Agency released the year-by-year global land-use dataset from 1992 to 2015 (Bontemps et al. 2013; Defourny et al. 2017). Since 2016, the Copernicus Climate Change Service (C3S) has released land cover data for 2016–2020, which are consistent with the global map series produced from 1992–2015 (Defourny et al. 2021). This dataset is the longest global land-use dataset in time series and is ideal for exploring large-scale land-use changes. The accuracy of this database is 74.1% (Defourny et al. 2017).

The CCI-LC legend contains 36 land cover classes. These categories are defined using the Land Cover Classification System (LCCS) developed by FAO (Di Gregorio 2005). This work reclassified the CCI-LC types to general types for clarity in analysis, referring to a general classification system (Gong et al. 2013). The original 36 classification and reclassification criteria are shown in Table 1.

Spatial change characterization

Land-use-transition analysis can describe the quantitative information of land-use changes, but this analysis cannot

Table 1 Correspondence between new land categories used for the change detection and the LCCS legend used in the CCI-LC classes

Reclassification		LCCS legend and its code number used in ESA-CCI LC maps	
Cropland	Rainfed cropland	10, 11, 12	Rainfed cropland
	Irrigated cropland	20	Irrigated cropland
	Mixed cropland	30	Mosaic cropland (>50%)/natural vegetation (tree, shrub, herbaceous cover) (<50%)
		40	Mosaic natural vegetation (tree, shrub, herbaceous cover) (>50%)/cropland (<50%)
Forest	Broadleaved forest	50	Tree cover, broadleaved, evergreen, closed to open (>15%)
		60, 61, 62	Tree cover, broadleaved, deciduous, closed to open (>15%)
	Needle-leaved forest	70, 71, 72	Tree cover, needle-leaved, evergreen, closed to open (>15%)
		80, 81, 82	Tree cover, needle-leaved, deciduous, closed to open (>15%)
	Mixed forest	90	Tree cover, mixed leaf type (broadleaved and needle-leaved)
		100	Mosaic tree and shrub (>50%)/herbaceous cover (<50%)
Grassland	Grassland	110	Mosaic herbaceous cover (>50%)/tree and shrub (<50%)
		130	Grassland
Wetland	Wetland	160	Tree cover, flooded, fresh or brackish water
		170	Tree cover, flooded, saline water
		180	Shrub or herbaceous cover, flooded, fresh-saline or brackish water
Urban	Urban	190	Urban areas
Shrubland	Shrubland	120, 121, 122	Shrubland
Bare area	Bare area (partly with sparse vegetation)	140	Lichens and mosses
		150,152,153,	Sparse vegetation (tree, shrub, herbaceous cover) (<15%)
		200,201,202	Bare areas
Water	Water	210	Water bodies
Ice	Ice and snow	220	Permanent snow and ice (stable)

analyze the spatial information of land-use changes. Given the fine resolution of CCI-LC, the land-use analysis at the world level will become too fragmented to capture variation characteristics. This work aggregates the original 300-m resolution into 10 km × 10 km cells (Li et al. 2018; Nowosad et al. 2019). This scale provides high resolution, enough to include meaningful feature analysis within each cell.

Each 10 km × 10 km grid contains multiple small grids of 300 m × 300 m. Here, the 'Statistics' function of ArcGIS software is used to calculate the changed area and the most dominant type of land-use change in each 10 km × 10 km grid. This paper proposes the ratio of the area of land-use change to the grid area of 10 km × 10 km, that is, the intensity of land-use change of each cell (Aldwaik and Pontius 2012). The calculation method is as follows:

$$\text{Proportion of land-use change} = \frac{\text{Land-use change area}}{\text{One cell size}} \times 100\% \quad (1)$$

Land-use change over time is measured by the difference in land use between the initial and final time (Nowosad et al. 2019). This work aims to explore the land-use change over the longest available period of time in the ESA dataset, that is, the 1992 and 2020 maps as the first- and last-time steps. The map was eventually classified into five levels, with percent change indicating the intensity of land-use change. A percentage above 30% is classified as "high change", a percentage between 15 and 30% is classified as "moderate high change", and a percentage between 5 and 15% is classified as "moderate change".

Results and discussion

Global karst land-use distribution map in 2020

The CCI-LC map in 2020 (reclassified according to Table 1) is combined with the WOKAM global karst area distribution map, as shown in Fig. 1. Figures 1 and 2 show the global karst land-use distribution map and proportion of each land-use type in 2020, respectively. About 8.54 million km^2 (31.78%) of the karst area is forest, which is also the land-use type with the largest proportion of global karst areas. Broadleaved forests are about 3.12 million km^2, accounting for 11.59%, whereby most are located in tropical climate zones—Southeast Asia, Latin America and Central Africa—and are mainly determined by climatic conditions (high temperature and precipitation). The area of needle-leaved forests is 4.25 million km^2 (15.82%),
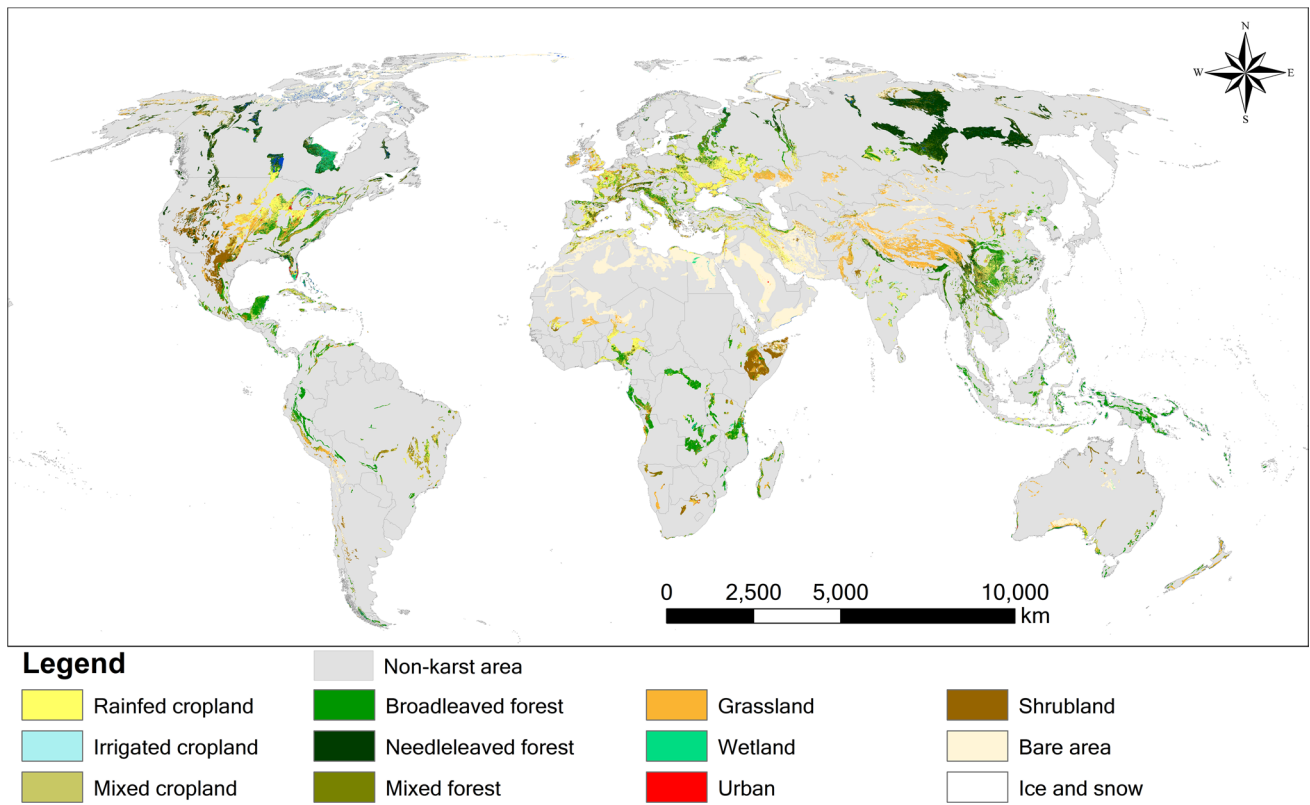
Fig. 1 Spatial patterns of global karst area land use in 2020, at 300-m spatial resolution. Data source: global karst distribution data from WOKAM (Chen et al. 2017a), land-use data from CCI-LC 2020 version (Defourny et al. 2021)

mainly distributed in the cold climate regions distributed in northern Russia and Canada, where the population density is very low (less than 20 people per km²). About 7.41 million km² (27.58%) of the global karst area is bare land, and
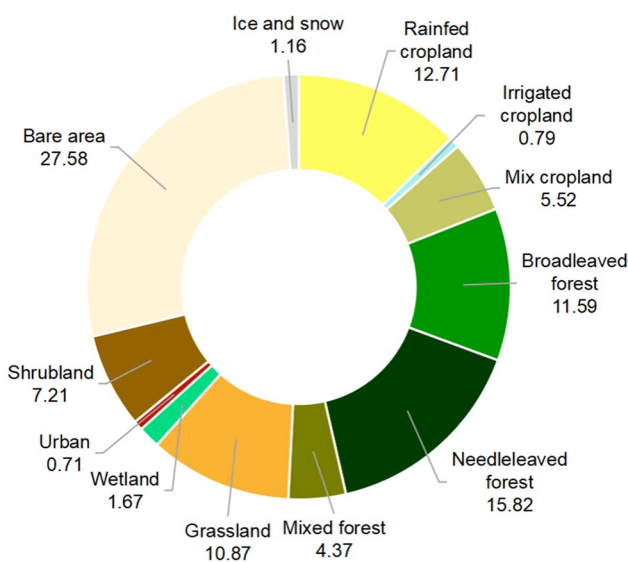
the most widespread bare land is distributed in the Arabian Peninsula and North Africa. Most of these areas have arid climates, where there are high temperatures combined with less rain. About 1.94 million km² (7.21%) are shrubland, which are distributed with bare land in the arid climate zone. Shrubs were suitable for revegetation in harsh karst areas because of high tolerance to severe drought compared to trees (Liu et al. 2011). Around 5.11 million km² (19.02%) of karst land is covered with cropland. Cropland is mainly distributed in the temperate climate areas, which is relatively warm with high precipitation amounts and seasonality. Rainfed cropland is mainly distributed in Europe, the eastern United States and other regions, with an area of about 3.42 million km² (12.71%). Irrigated cropland is about 0.21 million km² (0.79%). Although the area of irrigated cropland is relatively small, it represents managed landscapes with the highest agricultural inputs (Václavík et al. 2013). Concentrated irrigated agricultural areas are in regions such as China, Egypt and India. Grassland (10.87%) has less precipitation and is distributed in the central United States and Central Asia. The urban area is about 0.19 million km², accounting for about 0.71%. Urban areas with high-density population are scattered throughout the world.

Fig. 2 Pie chart of 2020 global karst area land use (unit: %)

Global change patterns

Land-use area change

The results of analysis of the area change of each land-use type over the 29-year period, from 1992 to 2020, are shown in Fig. 3 (numbers are in 10^3 km^2). Before 2000, the total amount of cropland increased, and then decreased year by year until 2017, followed by a minor increase from 2017 until 2018 and a stable period until 2020. Cropland referred to in the figure is the sum of rainfed cropland, irrigated cropland and mixed cropland. Globally, cropland area has been maintained at 5.11 million km^2, and two-thirds of the area is rainfed cropland. About half of the forests are needle-leaved forests, and after 2017 the area of needle-leaved forests has decreased sharply, accompanied by mixed forests that have been increasing over time. Such a sharp decline may be due to the classification of remote sensing data; some areas were classified as needle-leaved before 2017, and then classified

as mixed forest, but overall, forest is on the rise. The bare area shows a shrinking trend of 0.09 million km^2, about the size of Portugal. In contrast, the urban area increases gradually during the 28 years from 1992 to 2020, with an increase of 0.10 million km^2, which is about the size of the country of Iceland.

Land-use transition

Figure 4 illustrates land-use transition processes quantitatively between different types of global karst areas from 1992 to 2020. Net change shows the difference in areas of land use between 1992 and 2020 (see Table 2). Except for the category of snow and ice, all other land-use types experienced varying degrees of change in global karst area. Permanent snow and ice remained constant over the 29-year period (0.31 million km^2), mainly distributed in northern Canada and the Tibetan Plateau. This conclusion is different
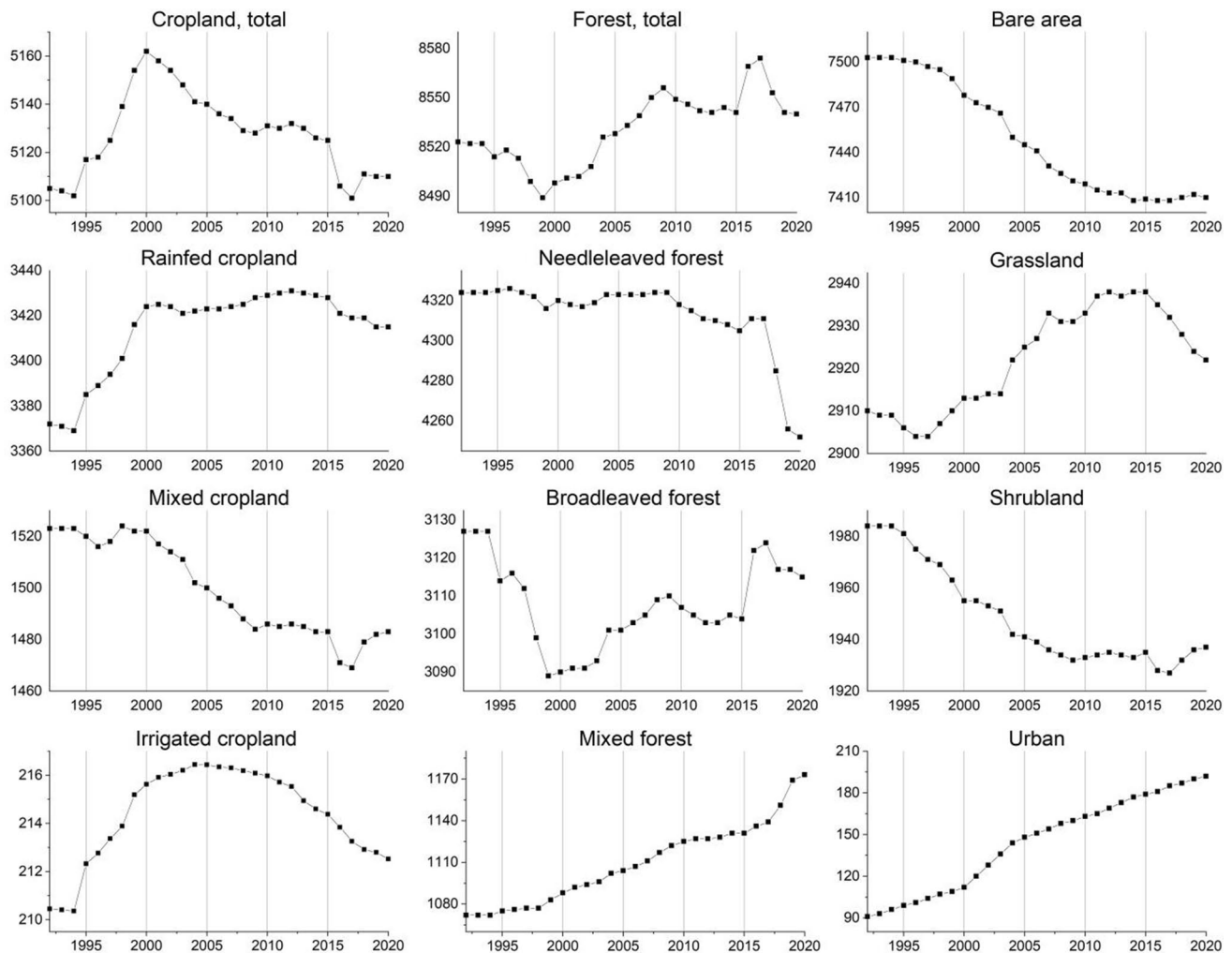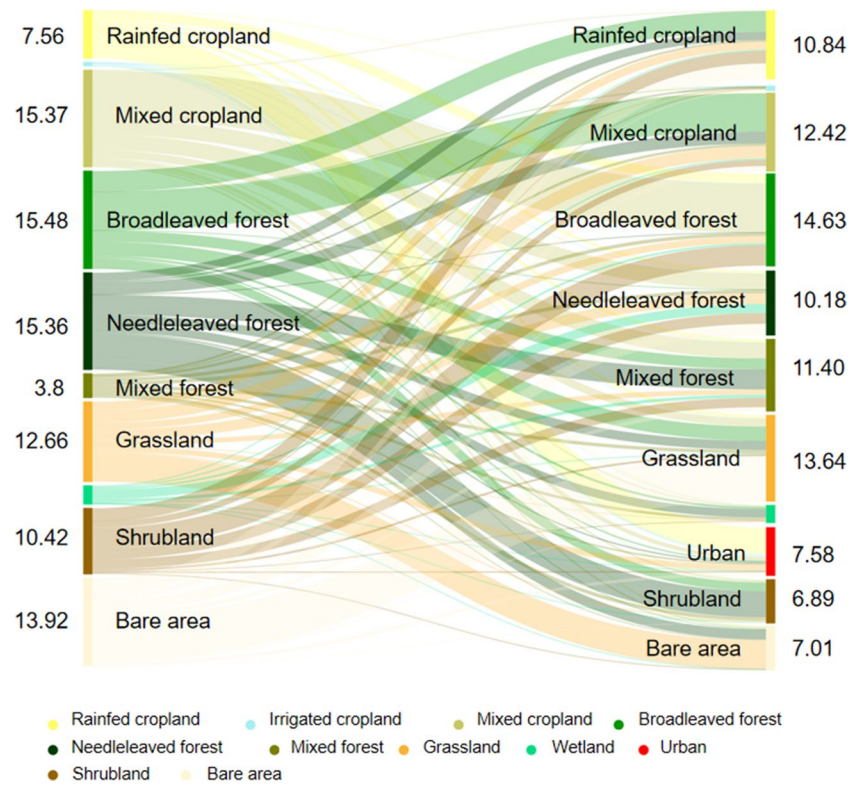

Fig. 3 Land-use area change in global karst regions from 1992 to 2020 (unit: 1,000 km^2)

Fig. 4 Transition of global karst land-use-change area from 1992 to 2020 (unit: %)

from that of Li et al. (2019), which may be due to different databases or data accuracy.

The total global karst area that experienced land-use changes from 1992 to 2020 is 1.30 million km^2, which means that almost 4.85% of the global karst surface has changed. Overall, the most frequent land-use changes occurred between cropland and forest; the largest land-use-change types were 'cropland to forest' and 'forest to cropland' with 0.20 million km^2 and 0.18 million km^2, respectively, accounting for 29.39% of all land-use changes on karst.

The total area of forest expansion is 17,400 km^2, with forest gains mainly coming from the annual growth of mixed

Table 2 Net change of different land-use types (unit: 10^3 km^2)

Land-use type	Net change
Rainfed cropland	43.41
Irrigated cropland	2.07
Mixed cropland	−40.37
Broadleaved forest	−11.87
Needle-leaved forest	−72.08
Mixed forest	101.35
Grassland	12.46
Wetland	−2.78
Urban	101.31
Shrubland	−47.11
Bare area	−92.94

forest (an increase of 0.10 million km^2). For broadleaved forests, the main gross loss was to mixed cropland and rainfed cropland amounting to 0.08 million and 0.04 million km^2, respectively. For needle-leaved forests, the main loss was to shrubland (0.05 million km^2), mixed forests (0.04 million km^2) and mixed cropland (0.02 million km^2).

Urbanization has received considerable attention due to economic development and dense population (Kalnay and Cai 2003). Globally, the area of change in urban areas is relatively small compared to other land-use changes. Urban areas have increased by 0.10 million km^2, accounting for 7.73% of the gross total global land-use change. The net increase in urban areas mainly comes from the conversion of cropland and grassland, amounting to 0.07 million and 0.01 million km^2, respectively. Cropland loss was mainly to forests and urban areas. In addition to turning cropland to forests, urban encroachment on cropland is also a key cause of cropland loss (Winfield 1973), indicating that the urban expansion caused by anthropogenic land usage from 1992 to 2020 was significant in the global karst regions.

Grassland also had an obvious transition to bare land; the loss of bare land cover was mainly to grassland (0.10 million km^2), rainfed cropland (0.03 million km^2) and needle-leaved forests (0.02 million km^2). The gain of bare areas was mainly coming from grasslands (0.06 million km^2) and needle-leaved forests (0.02 million km^2). Despite a gross bare-area gain of 0.09 million km^2, the larger gross loss (1.85 million km^2) results in a net loss of 0.09 million

km^2, which shows that grassland restoration is discernible in the karst area.

Spatial land-use change identification

Intensity of land-use change

In order to identify the spatial distribution of land-use change characteristics, the proportion of land-use change within each grid cell is calculated here according to Eq. (1). The spatial pattern of the proportion of land-use change in the global karst area is shown in Fig. 5. In all, 38.49% of the grid is 'no change', mainly distributed in northern North America, northern Africa and the Arabian Peninsula. The areas with more than 15% land-use change are mainly distributed in regions such as eastern North America, Central Europe and Southeast Asia, accounting for 9.92% of all karst areas, while areas with more than 30% land-use changes are distributed in Central America, Central Africa and South Asia, accounting for 2.70% of the total karst proportion. The tropical climate has a higher proportion of land-use change, and most of the regions with land-use change proportion of more than 30% are within this climate region.

Spatial distribution of the dominant type of land-use change

A variety of land-use change types occur in the global karst region from 1992 to 2020 within one cell. Figure 6 shows the distribution of the dominant type of land-use change. Land-use change usually has a high degree of spatial heterogeneity, which indicates that land-use change is related to local climatic factors and land-use planning, etc. (Liu et al. 2018).

Contrary to the prevailing view of global forest area decline, afforestation is the most common type of land-use change in global karst areas (Song et al. 2018), mainly distributed in North America, the east and west coasts of Africa, and southwest China. These shifts are related to changes in factors such as the 'Returning Farmland to Forest' program supported by local governments (Liu et al. 2015) or economically beneficial tree planting (Laikre et al. 2010; Hansen et al. 2013). Afforestation will improve the vegetation cover and decrease the loss of water and soil due to agricultural practices (Sahin and Hall 1996). This situation implies a greening trend due to a more suitable environment or increased precipitation in some areas (Song et al. 2018; Zhu et al. 2016).

Over the past few decades, agricultural reclamation areas have existed due to the expansion of cropland areas driven by growing populations (Tilman et al. 2011). Regions that contain significant cropland expansion are Southeast Asia,
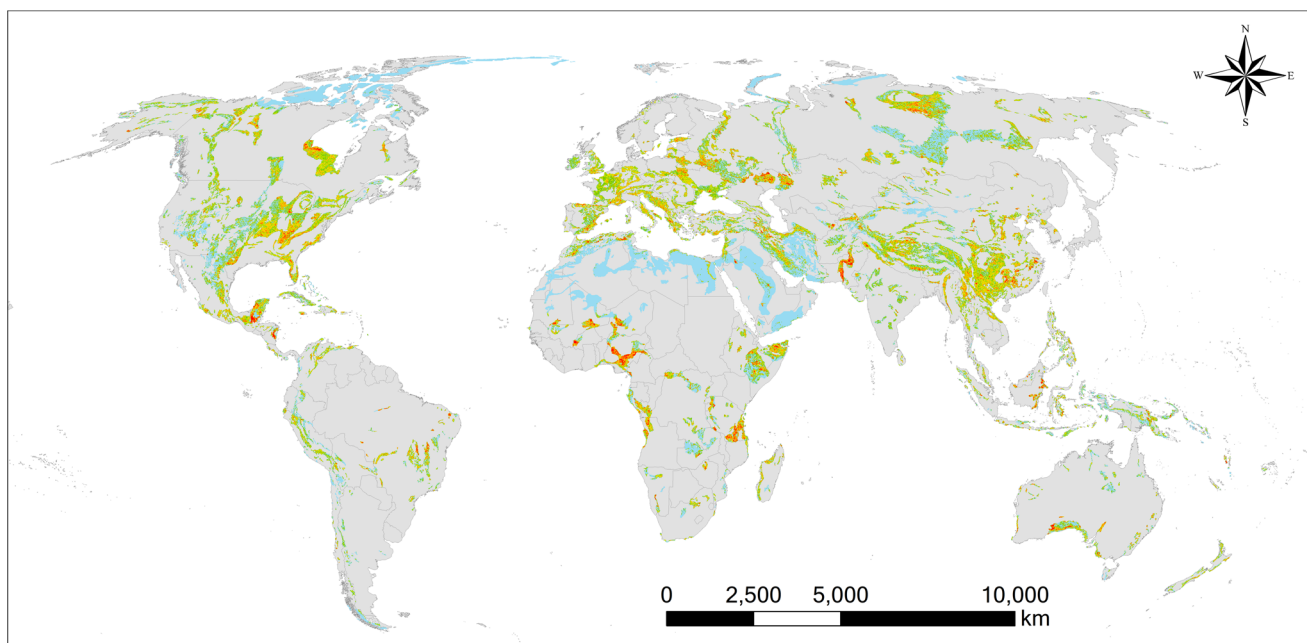
Legend

Proportion of land-use change

Non-karst area	< 2%	5% - 15%	> 30%
No change	2% - 5%	15% - 30%	

Fig. 5 Proportion of land-use change area in the 10 km × 10 km cells

Central Asia, and Central North America, as well as sporadic locations such as Latin America and Africa. Agricultural reclamation regions are highly consistent with the population density in karst regions (Goldscheider et al. 2020). In northern Africa, bare areas and shrublands encompassing several regions have been transformed into cropland expansion. In comparison, the southern region of Africa is mostly characterized by a conversion of forest into cropland.

The urbanization process leads to a range of environment-related issues (Lambin et al. 2001; Brown and Vivas 2005), including soil erosion, desertification, and water scarcity, etc. (Wang and Fang 2011). Urban expansion has occurred mainly in Central and Eastern Europe, the eastern regions of the USA, and sporadically in eastern China and the Arabian Peninsula. The most important land-use change involved in urban expansion is from rainfed cropland around the city.

Intense human activities have resulted in the karst rocky desertification landscape with extensive exposed bedrock, severe soil loss, shallow soil layers, and discontinuous soil coverage (Chen et al. 2021a, b). The main desertification areas of global karst areas are in the Tibetan Plateau, eastern North America and Central Russia. Among them, the karst areas in North America are dominated by the transformation from forest into shrubland, while in Tibet and Russia, grassland is mainly degraded into bare area.

Detailed analyses of land-use change in three sample areas

The karst regions of south-central Europe, eastern North America and southwest China are the three major karst concentrations in the world (Yuan 1999). In this study, locations with a large proportion of land-use change in the global karst concentration area are selected as samples: in the eastern United States (A), southeastern Spain (B) and central south China (C). A location map of the selected sample areas, and the corresponding proportions of land-use change and the dominant type of land-use change maps, are shown in Fig. 7.

Sample area A is in the Eastern United States. The USA is the second largest karst water consumer, where approximately 50 million people (Stevanović 2019) are supplied with drinking water from karst. Sample area A is located in the eastern United States, on the borders of Kentucky, Indiana and Ohio, most of which rely on karst groundwater. The map shows an area within the state of Indiana where the proportion of land-use change exceeds 30%. The dominant type of land-use change is cropland to urban, indicating that urban expansion is significant in Indiana and Ohio (Lawler et al. 2014). Large-scale urban expansion will lead to the depletion of natural vegetation within protected areas (Martinuzzi et al. 2015). The area south of the sample shows not only urban expansion, but also forest deforestation and agricultural reclamation.
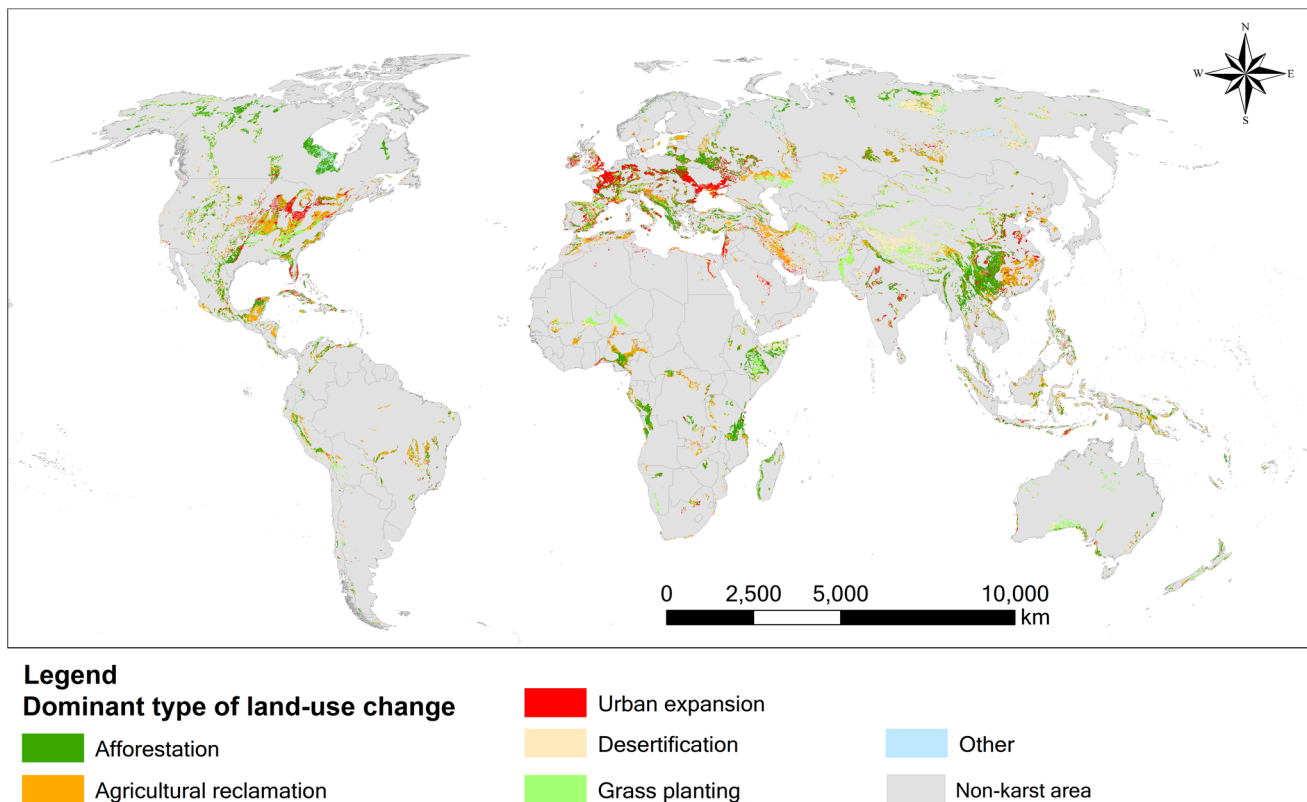

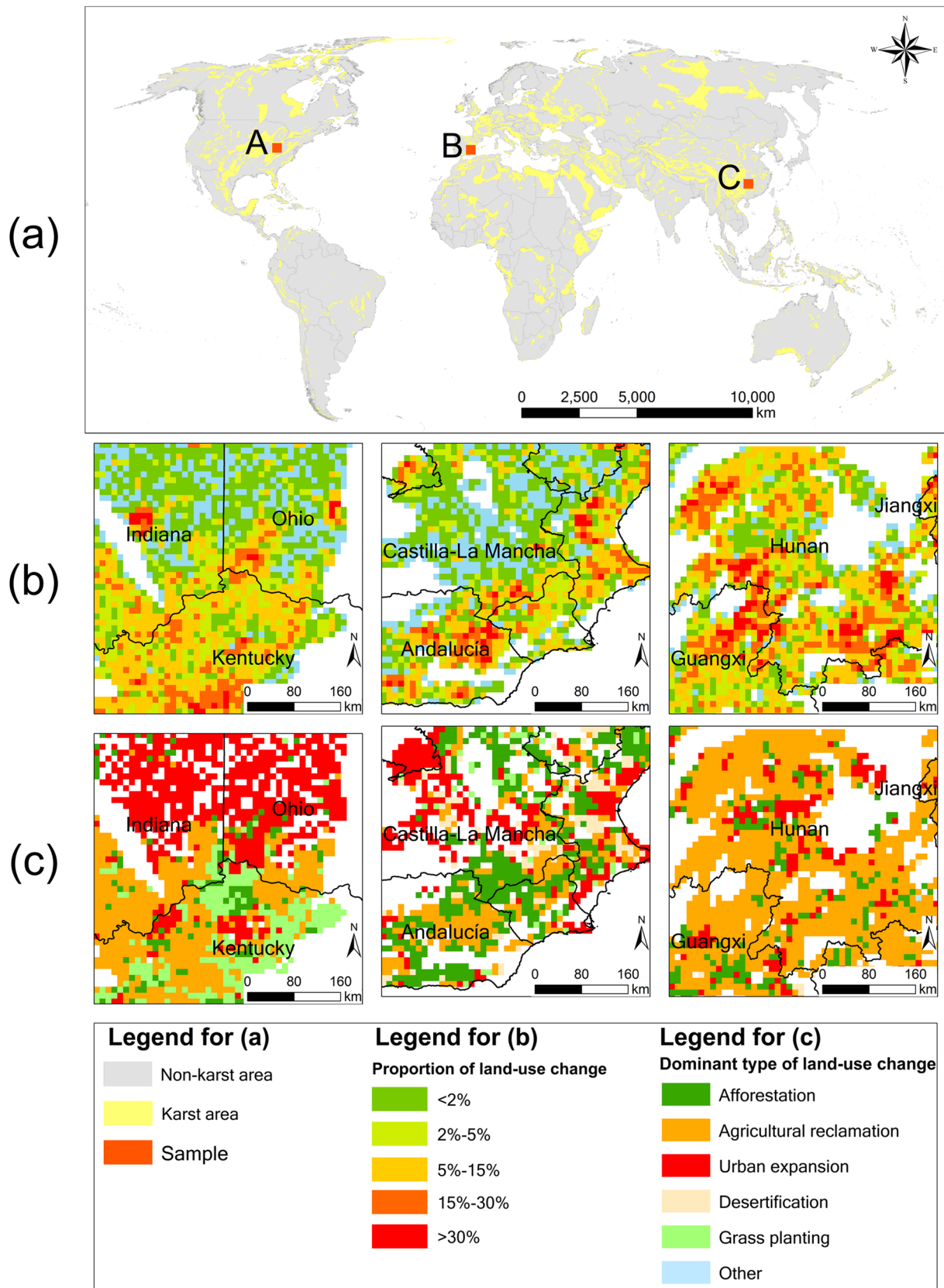**Fig. 6** The dominant type of land-use change in the 10 km × 10 km cells

Fig. 7 Land-use changes between 1992 and 2020 for three karst areas: eastern United States (A), southeastern Spain (B, and central south China (C), showing **a** global karst distribution map and sample sites, (**b**) proportion of land-use change, and (**c**) dominant type of land-use change

Sample area B is located in southeastern Spain, Valencia and its northern regions. The main land-use change type is intense afforestation and agricultural reclamation, with urbanization around the cities. In the central and southern parts, this area of agriculture is dense rainfed cropland, and the main land use is bare area. Trends in land-use change also include the expansion of irrigated crop systems (Serra et al. 2014). Urban expansion in the northern part mainly comes from urban encroachment on cropland. The gradual conversion of traditional agriculture into forestry or intensive farming has been driven by agricultural and socio-economic policies (Hewitt and Escobar 2011).

Sample area C is located in central south China, which has a large continuous distribution of ecologically fragile karst areas (Jiang et al. 2014; Bai et al. 2013). At the same time, there are vegetation degradation and rocky desertification in the karst region of South China (Liao et al. 2018). Sample area C shows the highest proportion of land-use change among the three samples. The most common type of land-use change is forest to cropland as well as a shrubland-to-cropland type of change. Land policy has promoted cropland expansion (Peng et al. 2011), which is associated with dense population in the southwestern karst areas of China. Agriculture in the region is dominated by irrigated cropland and mixed cropland which will lead to erosion in karst areas (Liu et al. 2014).

Conclusion

This paper represents the first attempt to combine two global datasets for analysis and comparison. The study utilized CCI-LC data and WOKAM data from 1992 to 2020 to identify and quantify land-use changes and distribution patterns in global karst areas. The availability of these datasets describing the global karst distribution and land-use change has enabled the first quantification of land-use change in karst regions at a global scale. The main findings and conclusions can be summarized as follows:

In 2020, around 8.54 million km^2 (31.78%) of the global karst areas are forest, about half of which is needle-leaved forest. About 5.11 million km^2 (19.02%) of karst areas are covered with cropland, which can be further divided into rainfed cropland (12.71%), irrigated cropland (0.79%) and mixed cropland (5.52%). Bare areas and grasslands accounted for 27.58% and 10.87%, respectively. The urban area is 0.19 million km^2 (0.71%).

The area of land-use changes in global karst areas from 1992 to 2020 is 1.30 million km^2, which means that almost 4.85% of the global karst surface has changed. Most of the changes occurred in the conversion between forest and cropland, accounting for 29.39% of all land-use changes on karst. The net increase in urban areas is 0.1 million km^2, with most

of the expansion coming from rainfed croplands. In contrast, the bare areas and shrublands have been shrinking by about 0.09 million and 0.05 million km^2, respectively.

This paper proposes two indicators—land-use-change proportion and a dominant type of land-use change—in $10\ km \times 10\ km$ cells to identify the characteristics of land-use change in karst regions. The areas with more than 15% land-use change are mainly distributed in eastern North America, Central Europe and Southeast Asia, accounting for 9.92% of all karst areas. The tropical climate regions have a higher proportion of land-use change. In addition, when exploring the characteristics of land-use change in global karst areas, it is found that the land-use change is dominated by forest expansion, accompanied by sporadic urbanization and agricultural reclamation. These agricultural reclamation regions are highly consistent with higher population density, mainly concentrated in China, Europe and North America.

These results reflect the current status and distribution of global karst land use, showing land-use transition over the last 29 years. Continuous satellite observation will provide a basis of evidence for understanding land use and its change at the global scale. Human activities and climate change directly or indirectly affected land use. Traces of land-use change by human activities have been found in large areas of every continent. It is necessary to pay continuous attention to the impact of karst land use on karst groundwater resources.

Declarations

References

Aldwaik SZ, Pontius RG Jr (2012) Intensity analysis to unify measurements of size and stationarity of land changes by interval, category, and transition. Landsc Urban Plan 106(1):103–114

Bai XY, Wang SJ, Xiong KN (2013) Assessing spatial-temporal evolution processes of karst rocky desertification land: indications for restoration strategies. Land Degrad Dev 24(1):47–56

Bartholome E, Belward AS (2005) GLC2000: a new approach to global land cover mapping from Earth observation data. Int J Remote Sens 26(9):1959–1977

Bontemps S, Defourny P, Radoux J, Van Bogaert E, Lamarche C, Achard F, Mayaux P, Boettcher M, Brockmann C, Kirches G, Zülkhe M, Kalogirou V, Seifert FM, Arino O (2013). Consistent global land cover maps for climate modelling communities: current achievements of the ESA's land cover CCI. In: Proceedings of the ESA living planet symposium, vol 13, Edinburgh, September 2013, pp 9–13

Brown MT, Vivas MB (2005) Landscape development intensity index. Environ Monit Assess 101(1):289–309

Chen J, Chen J, Liao A, Cao X, Chen L, Chen X, He C, Han G, Peng S, Lu M, Zhang W, Tong X, Mills J (2015) Global land cover mapping at 30 m resolution: a POK-based operational approach. ISPRS J Photogramm Remote Sens 103:7–27

Chen F, Wang S, Bai X, Liu F, Zhou D, Tian Y, Luo G, Li Q, Wu L, Zheng C, Xiao J, Qian Q, Cao Y, Li H, Wang M, Yang Y (2021a) Assessing spatial-temporal evolution processes and driving forces of karst rocky desertification. Geocarto Int 36(3):262–280

Chen W, Zhang X, Huang Y (2021b) Spatial and temporal changes in ecosystem service values in karst areas in southwestern China based on land use changes. Environ Sci Pollut Res 28:45724–45738

Chen Z, Auler AS, Bakalowicz M, Drew D, Griger F, Hartmann J, Jiang G, Moosdorf N, Richts A, Stevanovic Z, Veni G, Goldscheider N (2017a) The world karst aquifer mapping project: concept, mapping procedure and map of Europe. Hydrogeol J 25(3):771–785

Chen Z, Goldscheider N, Auler AS, Bakalowicz M, Broda S, Drew D, Hartmann J, Jiang G, Moosdorf N, Richts A, Stevanovic Z, Veni G, Dumont A, Aureli A, Clos P, Krombholz M (2017b) World Karst Aquifer Map (WHYMAP WOKAM). BGR, IAH, KIT, UNESCO. https://doi.org/10.25928/b2.21_sfkq-r406

Defourny P, Bontemps S, Lamarche C, Brockmann C, Boettcher M, Wevers J, Kirches G (2017) Land Cover CCI: product user guide version 2.0. http://maps.elie.ucl.ac.be/CCI/viewer/. Accessed June 2013

Defourny P, Lamarche C, Marissiaux Q, Brockmann C, Boettcher M, Kirches G (2021) Product user guide and specification, ICDR Land Cover 2016-2020. Ref. D5.3.1_PUGS_ICDR_LC_v2.1.x_PRODUCTS_v1.1. https://datastore.copernicus-climate.eu/documents/satellite-land-cover/D5.3.1_PUGS_ICDR_LC_v2.1.x_PRODUCTS_v1.1.pdf. Accessed June 2013

DeFries R (2013) Why forest monitoring matters for people and the planet. In: Global forest monitoring from Earth observation, Routledge, London, pp 1–14

Di Gregorio A (2005) Land cover classification system: classification concepts and user manual: LCCS, vol 2. FAO, Rome

Foley JA, DeFries R, Asner GP, Barford C, Bonan G, Carpenter SR, Chapin FS, Coe MT, Daily GC, Gibbs HK, Helkowski JH, Holloway T, Howard EA, Kucharik CJ, Monfreda C, Patz JA, Prentice IC, Ramankutty N, Snyder PK (2005) Global consequences of land use. Science 309(5734):570–574

Foley JA, Ramankutty N, Brauman KA, Cassidy ES, Gerber JS, Johnston M, Mueller ND, O'Connell C, Ray DK, West PC, Balzer C, Bennett EM, Carpenter SR, Hill J, Monfreda C, Polasky S, Rockström J, Sheehan J, Siebert S, Tilman D, Zaks DP (2011) Solutions for a cultivated planet. Nature 478(7369):337–342

Friedl MA, Sulla-Menashe D, Tan B, Schneider A, Ramankutty N, Sibley A, Huang X (2010) MODIS Collection 5 global land cover: algorithm refinements and characterization of new datasets. Remote Sens Environ 114(1):168–182

Fuchs R, Herold M, Verburg PH, Clevers JG (2013) A high-resolution and harmonized model approach for reconstructing and analysing historic land changes in Europe. Biogeosciences 10(3):1543–1559

Goldscheider N (2019) A holistic approach to groundwater protection and ecosystem services in karst terrains. Carbon Evapor 34(4):1241–1249

Goldscheider N, Chen Z, Auler AS, Bakalowicz M, Broda S, Drew D, Hartmann J, Jiang G, Moosdorf N, Stevanovic Z, Veni G (2020) Global distribution of carbonate rocks and karst water resources. Hydrogeol J 28(5):1661–1677

Gong P, Wang J, Yu L, Zhao Y, Zhao Y, Liang L, Niu Z, Huang X, Fu H, Liu S, Li C, Li X, Fu W, Liu C, Xu Y, Wang X, Cheng Q, Hu L, Yao W, Zhang H, Zhu P, Zhao Z, Zhang H, Zheng Y, Ji L, Zhang Y, Chen H, Yan A, Guo J, Yu L, Wang L, Liu X, Shi T, Zhu M, Chen Y, Yang G, Tang P, Xu B, Giri C, Clinton N, Zhu Z, Chen J, Chen J (2013) Finer resolution observation and monitoring of global land cover: first mapping results with Landsat TM and ETM+ data. Int J Remote Sens 34(7):2607–2654

Grekousis G, Mountrakis G, Kavouras M (2015) An overview of 21 global and 43 regional land-cover mapping products. Int J Remote Sens 36(21):5309–5335

Grimm NB, Faeth SH, Golubiewski NE, Redman CL, Wu J, Bai X, Briggs JM (2008) Global change and the ecology of cities. Science 319(5864):756–760

Hansen MC, Potapov PV, Moore R, Hancher M, Turubanova SA, Tyukavina A, Thau D, Stehman SV, Goetz SJ, Loveland TR, Kommareddy A, Egorovl A, Chini L, Justice CO, Townshend JRD (2013) High-resolution global maps of 21st-century forest cover change. Science 342(6160):850–853

Hartmann A, Goldscheider N, Wagener T, Lange J, Weiler M (2014) Karst water resources in a changing world: review of hydrological modeling approaches. Rev Geophys 52(3):218–242

Hewitt R, Escobar F (2011) The territorial dynamics of fast-growing regions: unsustainable land use change and future policy challenges in Madrid, Spain. Appl Geogr 31(2):650–667

Jiang Z, Lian Y, Qin X (2014) Rocky desertification in Southwest China: impacts, causes, and restoration. Earth Sci Rev 132:1–12

Kalnay E, Cai M (2003) Impact of urbanization and land-use change on climate. Nature 423(6939):528–531

Laikre L, Schwartz MK, Waples RS, Ryman N, GeM Working Group (2010) Compromising genetic diversity in the wild: unmonitored large-scale release of plants and animals. Trends Ecol Evol 25(9):520–529

Lambin EF, Turner BL, Geist HJ, Agbola SB, Angelsen A, Bruce JW, Coomes OT, Dirzo R, Fischer G, Folke C, George PS, Homewood K, Imbernon J, Leemans R, Li X, Moran EF, Mortimore M, Ramakrishnan PS, Richards JF, Skanes H, Steffent W, Stone GD, Svedin U, Veldkamp TA, Vogel C, Xu J (2001) The causes of land-use and land-cover change: moving beyond the myths. Glob Environ Chang 11(4):261–269

Lawler JJ, Lewis DJ, Nelson E, Plantinga AJ, Polasky S, Withey JC, Helmers DP, Martinuzzi S, Pennington D, Radeloff VC (2014) Projected land-use change impacts on ecosystem services in the United States. Proc Natl Acad Sci 111(20):7492–7497

Li W, MacBean N, Ciais P, Defourny P, Lamarche C, Bontemps S, Houghton RA, Peng S (2018) Gross and net land cover changes in the main plant functional types derived from the annual ESA CCI land cover maps (1992–2015). Earth Syst Sci Data 10(1):219–234

Li YJ, Ding YJ, Shangguan DH, Wang RJ (2019) Regional differences in global glacier retreat from 1980 to 2015. Adv Clim Chang Res 10(4):203–213

Liao C, Yue Y, Wang K, Fensholt R, Tong X, Brandt M (2018) Ecological restoration enhances ecosystem health in the karst regions of southwest China. Ecol Ind 90:416–425

Liu CC, Liu YG, Guo K, Li GQ, Zheng YR, Yu LF, Yang R (2011) Comparative ecophysiological responses to drought of two shrub and four tree species from karst habitats of southwestern China. Trees 25(3):537–549

Liu J, Liu M, Zhuang D, Zhang Z, Deng X (2003) Study on spatial pattern of land-use change in China during 1995–2000. Sci China Ser D Earth Sci 46(4):373–384

Liu L, Xu X, Liu J, Chen X, Ning J (2015) Impact of farmland changes on production potential in China during 1990–2010. J Geog Sci 25(1):19–34

Liu X, Yu L, Si Y, Zhang C, Lu H, Yu C, Gong P (2018) Identifying patterns and hotspots of global land cover transitions using the ESA CCI Land Cover dataset. Remote Sens Lett 9(10):972–981

Liu Y, Huang X, Yang H, Zhong T (2014) Environmental effects of land-use/cover change caused by urbanization and policies in Southwest China Karst area: a case study of Guiyang. Habitat Int 44:339–348

Loveland TR, Reed BC, Brown JF, Ohlen DO, Zhu Z, Yang LW, Merchant JW (2000) Development of a global land cover characteristics database and IGBP DISCover from 1 km AVHRR data. Int J Remote Sens 21(6–7):1303–1330

Martinuzzi S, Radeloff VC, Joppa LN, Hamilton CM, Helmers DP, Plantinga AJ, Lewis DJ (2015) Scenarios of future land use change around United States' protected areas. Biol Cons 184:446–455

Meyfroidt P, Lambin EF, Erb KH, Hertel TW (2013) Globalization of land use: distant drivers of land change and geographic displacement of land use. Curr Opin Environ Sustain 5(5):438–444

Misra A, Balaji R (2015) A study on the shoreline changes and land-use/land-cover along the South Gujarat coastline. Proc Eng 116:381–389

Nguyet VT, Goldscheider N (2006) A simplified methodology for mapping groundwater vulnerability and contamination risk, and its first application in a tropical karst area, Vietnam. Hydrogeol J 14(8):1666–1675

Nowosad J, Stepinski TF, Netzel P (2019) Global assessment and mapping of changes in mesoscale landscapes: 1992–2015. Int J Appl Earth Obs Geoinf 78:332–340

Panagopoulos A, Giannika V (2022) Comparative techno-economic and environmental analysis of minimal liquid discharge (MLD) and zero liquid discharge (ZLD) desalination systems for seawater brine treatment and valorization. Sustain Energy Technol Assess 53:102477

Parise M, Closson D, Gutiérrez F, Stevanović Z (2015) Anticipating and managing engineering problems in the complex karst environment. Environ Earth Sci 74(12):7823–7835

Peng J, Xu YQ, Cai YL, Xiao HL (2011) The role of policies in land use/cover change since the 1970s in ecologically fragile karst areas of Southwest China: a case study on the Maotiaohe watershed. Environ Sci Policy 14(4):408–418

Sahin V, Hall MJ (1996) The effects of afforestation and deforestation on water yields. J Hydrol 178(1–4):293–309

Serra P, Vera A, Tulla AF, Salvati L (2014) Beyond urban–rural dichotomy: exploring socioeconomic and land-use processes of change in Spain (1991–2011). Appl Geogr 55:71–81

Song XP, Hansen MC, Stehman SV, Potapov PV, Tyukavina A, Vermote EF, Townshend JR (2018) Global land change from 1982 to 2016. Nature 560(7720):639–643

Sonter LJ, Moran CJ, Barrett DJ, Soares-Filho BS (2014) Processes of land use change in mining regions. J Clean Prod 84:494–501

Stevanović Z (2019) Karst waters in potable water supply: a global scale overview. Environ Earth Sci 78(23):1–12

Tateishi R, Uriyangqai B, Al-Bilbisi H, Ghar MA, Tsend-Ayush J, Kobayashi T, Kasimu A, Hoan NT, Shalaby A, Alsaaideh B, Enkhzaya T, Gegentana SHP (2011) Production of global land cover data–GLCNMO. Int J Digit Earth 4(1):22–49

Tilman D, Balzer C, Hill J, Befort BL (2011) Global food demand and the sustainable intensification of agriculture. Proc Natl Acad Sci 108(50):20260–20264

Turner BL, Janetos AC, Verbug PH, Murray AT (2013) Land system architecture: using land systems to adapt and mitigate global environmental change (No. PNNL-SA-93482). Pacific Northwest National Lab, Richland, WA

Václavík T, Lautenbach S, Kuemmerle T, Seppelt R (2013) Mapping global land system archetypes. Glob Environ Chang 23(6):1637–1647

Wang J, Fang C (2011) Growth of urban construction land: progress and prospect. Prog Geogr 30(11):1440–1448

Ward D, Phinn SR, Murray AT (2000) Monitoring growth in rapidly urbanizing areas using remotely sensed data. Prof Geogr 52(3):371–386

Winfield D (1973) Function minimization by interpolation in a data table. IMA J Appl Math 12(3):339–347

Winkler K, Fuchs R, Rounsevell M, Herold M (2021) Global land use changes are four times greater than previously estimated. Nat Commun 12(1):1–10

Yuan D (1999) Progress in the study on karst processes and carbon cycle (in Chinese). Adv Earth Sci 14(5)

Zhu Z, Piao S, Myneni RB, Huang M, Zeng Z, Canadell JG, Ciais P, Sitch S, Friedlingstein P, Arneth A, Cao C, Cheng L, Kato E, Koven C, Li Y, Lian X, Liu Y, Liu R, Mao J, Pan Y, Peng S, Peñuelas J, Poulter B, Pugh TAM, Stocker BD, Viovy N, Wang X, Wang Y, Xiao Z, Yang H, Zaehle S, Zeng N (2016) Greening of the Earth and its drivers. Nat Clim Chang 6(8):791–795